

Molecular cation and low-dimensional perovskite surface passivation in perovskite solar cells

Received: 22 February 2023

Sam Teale  ^{1,4,6}, Matteo Degani  ^{2,6}, Bin Chen  ^{1,3}, Edward H. Sargent  ^{1,3,5}  & Giulia Grancini  ² 

Accepted: 22 March 2024

Published online: 4 July 2024

 Check for updates

The deposition of large ammonium cations onto perovskite surfaces to passivate defects and reduce contact recombination has enabled exceptional efficiency and stability in perovskite solar cells. These ammonium cations can either assemble as a thin molecular layer at the perovskite surface or induce the formation of a low-dimensional (usually two-dimensional) perovskite capping layer on top of the three-dimensional perovskite. The formation of these two different structures is often overlooked by researchers, although they impact differently on device operation. In this Review, we seek to distinguish between these two passivation layers. We consider the conditions needed for the formation of low-dimensional perovskite and the electronic properties of the two structures. We discuss the mechanisms by which each method improves photovoltaic efficiency and stability. Finally, we summarize the knowledge gaps that need to be addressed to better understand and optimize ammonium cation-based passivation strategies.

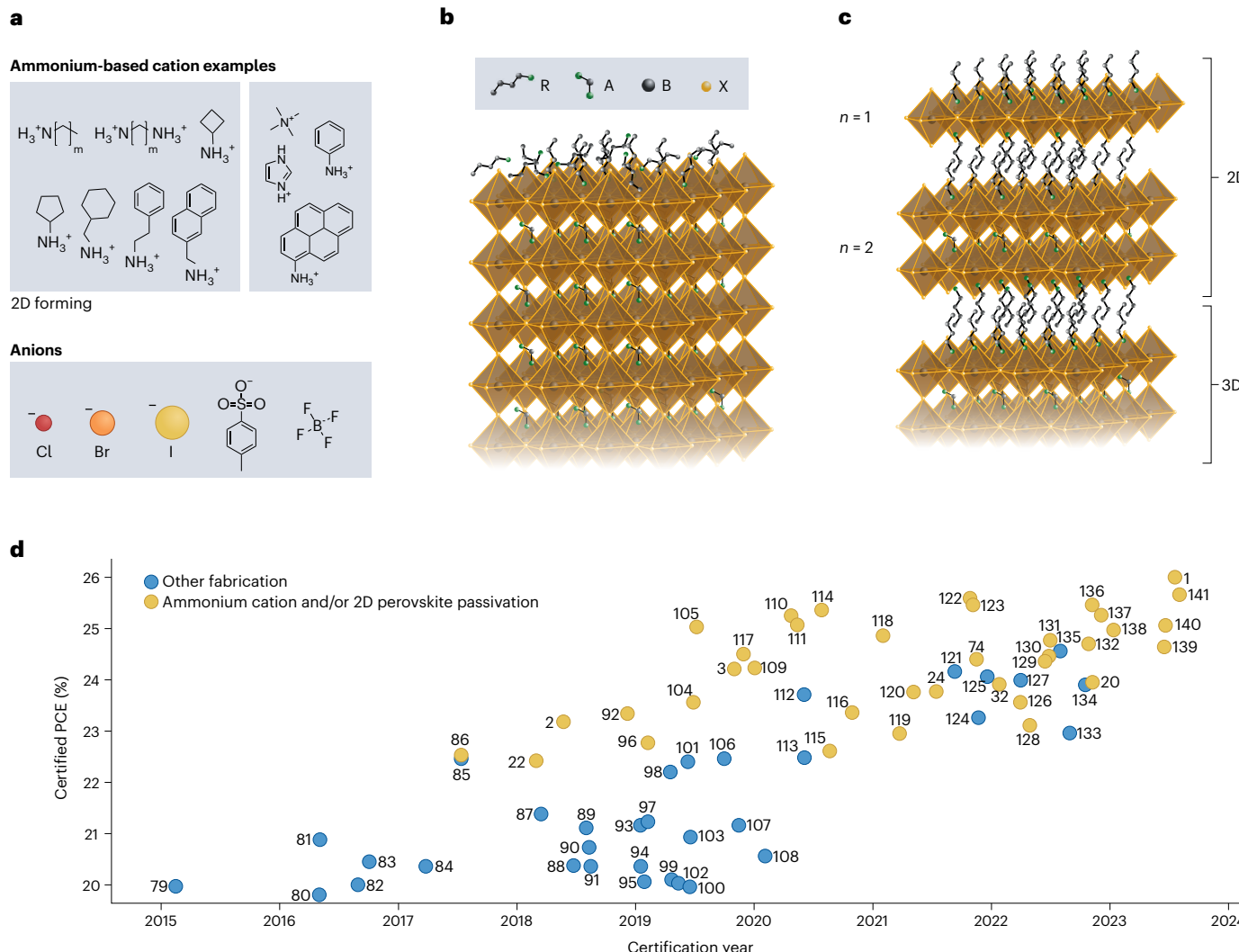
Perovskite solar cells (PSCs) have achieved power conversion efficiencies (PCEs) of >26%¹, attracting the attention of photovoltaics manufacturers. Recent improvements in efficiency have been enabled by the passivation of trap states at the surface of the perovskite film or at the interface between the perovskite and contact layers². Generally surface passivation layers are deposited using solution processing, but they can be evaporated or physically stacked. The most widely used materials to passivate perovskite film surfaces are ammonium ligand salts with alkylammonium chains, cyclic or aromatic ammonium cations and typically a halide anion (Fig. 1a). Ammonium cations in these salt solutions can bind to the perovskite surface via A-site vacancies or hydrogen bonding, forming a thin molecular layer on top of the perovskite (Fig. 1b). However, under some conditions (discussed herein), these large ammonium cations can also transform the surface of three-dimensional (3D) perovskite, replacing the A site to form

low-dimensional perovskite structures, most commonly 2D perovskite (Fig. 1c). 2D perovskite is obtained by slicing the 3D perovskite along its inorganic planes. A layered system is formed where inorganic layers are spaced by large organic cations with the structure $R_2A_{n-1}Pb_nI_{3n+1}$, where R is the spacer cation, A is the A site to a 3D perovskite and n is the number of 3D perovskite units sandwiched between the bulky ligands, defining the so-called dimensionality of the system. These structures can be purely 2D ($n = 1$) or quasi-2D ($n \geq 2$). For simplicity herein, both are referred to generically as 2D perovskite unless distinction between the two structures is required.

Figure 1d shows that the vast majority of PSCs with certified efficiencies above 23% PCE use a 2D or molecular cation passivation layer based on ammonium cations. For most of these entries, a detailed analysis of the passivation layer was not provided; thus, it is unclear whether a 2D passivation layer, a molecular cation passivation layer

¹The Edward S. Rogers Sr. Department of Electrical and Computer Engineering, University of Toronto, Toronto, Ontario, Canada. ²Department of Chemistry and INSTM, Università di Pavia, Pavia, Italy. ³Department of Chemistry, Northwestern University, Evanston, IL, USA. ⁴Present address: Clarendon Laboratory, University of Oxford, Oxford, UK. ⁵Department of Electrical and Computer Engineering, Northwestern University, Evanston, IL, USA.

⁶These authors contributed equally: Sam Teale, Matteo Degani.  e-mail: ted.sargent@northwestern.edu; giulia.grancini@unipv.it



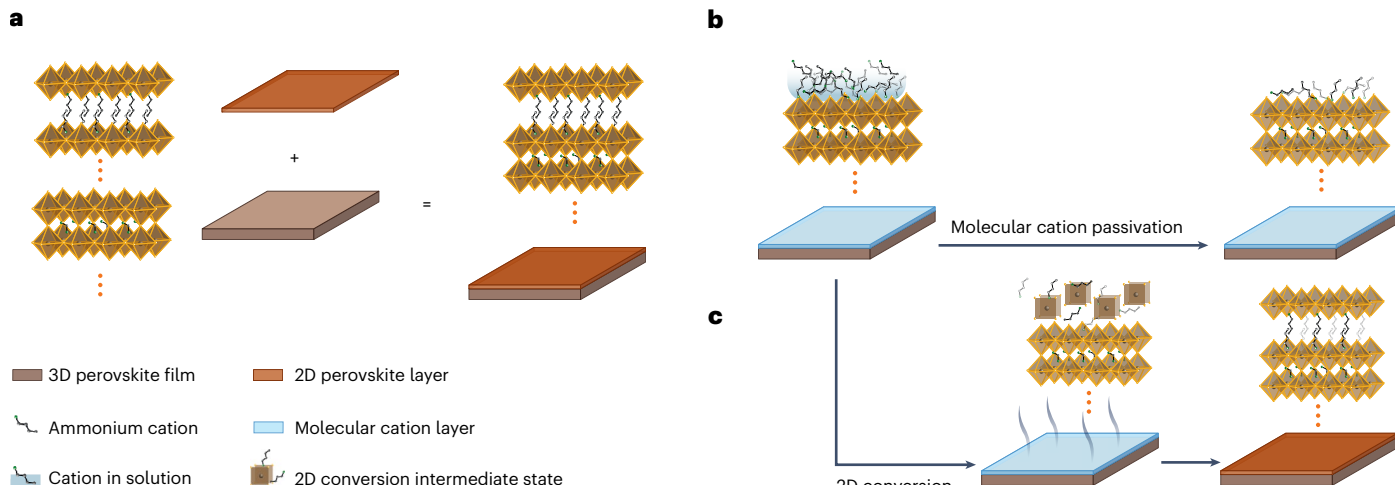


Fig. 2 | Fabrication methods to produce a 2D or molecular cation passivation layer. **a**, Direct fabrication using pre-made 2D perovskite deposited atop 3D perovskite to form a 2D/3D heterostructure. **b,c**, Indirect fabrication where ammonium cations are deposited onto a 3D perovskite surface and

either no conversion occurs and a molecular cation passivation layer forms (**b**) or conversion from 3D to 2D perovskite takes place to form a 2D/3D heterostructure (**c**).

molecular cation layers. However, due to quantum confinement, 2D perovskite produces distinct photoluminescence compared with 3D perovskite; thus, it is easier to determine the conformality of a 2D passivation layer. The conformality of either passivation layer is important as it affects both efficiency (through band alignment and charge extraction) and stability (through ion blocking and moisture protection).

Some fabrication methods generate an unambiguous result (that is, the direct deposition of a pre-made 2D perovskite will form a conformal 2D/3D heterostructure, whereas the deposition of an ammonium ligand that cannot form a 2D perovskite will produce a molecular passivation layer). Uncertainty arises when using indirect methods with ammonium ligands that can form 2D perovskite: conflicting reports in the literature suggest that either a 2D perovskite or a molecular layer can form depending on the processing conditions. For example, phenethylammonium iodide (PEAI) can generate a 2D perovskite in the form of PEA_2PbI_4 . However, once a PEAI solution is coated onto a 3D perovskite surface, some studies show that a 2D phase forms spontaneously⁵, whereas others find that 2D perovskite forms only if the film is heated². Many reports use a PEAI treatment (or similar) without investigating whether 2D perovskite is present; thus, a general ambiguity exists around how 2D passivation layers or molecular cation passivation layers affect device physics.

Additionally, as mentioned above, even if the 2D perovskite is visible in photoluminescence measurements it is not necessarily a conformal layer. Hyperspectral photoluminescence images of 3D perovskite films treated with ammonium ligands from Ugur et al.⁶ reveal that 2D perovskite may form conformally or in a discontinuous manner (Fig. 3b,e,h). This is supported by transmission electron microscopy images from other studies (Fig. 3c,f,i). Thus, to compare molecular cation and 2D perovskite passivation, we must first describe the parameters that control the formation of 2D perovskite, after which we can focus on reports that clearly distinguish between 2D passivation layers and molecular cation passivation layers. Here we consider reports that show conformal 2D layers only, as other reports may have non-conformal layers that are probably a mix of 2D and molecular cation passivation (as in Fig. 3b); thus, it is difficult to distinguish between each passivation type. The conformality of molecular cation layers is difficult to determine, but these layers are distinct from 2D passivation layers and thus a useful comparison is possible.

Conditions required to form 2D perovskite passivation layers

Density functional theory calculations consistently show that the formation energy of 2D perovskite is lower than that of a 3D structure: this drives the conversion from 3D to 2D upon exposure of 3D perovskite to 2D cations⁷. 2D cations bisect slabs of 3D perovskite as there is increasing thermodynamic favourability to replace 3D cation-terminated perovskite with 2D cation-terminated perovskite⁵.

Whether a spacer cation can form 2D perovskite has been extensively studied by Kanatzidis and colleagues⁸ who examined formation in solution with other perovskite precursors. They suggest that the propensity for 2D perovskite to form is governed by six factors (spacer charge, shape, size, solubility, hydrogen bonding and reactivity): (1) the spacer charge must be 1+ to form a Ruddlesden–Popper structure or 2+ to form a Dion–Jacobson structure; (2) there is an increasing chance of formation for ligands with decreased steric hindrance around the ammonium group ($\text{RNH}_3^+ > \text{R}_2\text{NH}_2^+ > \text{R}_3\text{NH}^+ > \text{R}_4\text{N}^+$, where R is an alkyl chain or other functional group); (3) there is a requirement for a chain length of ≥ 3 and ≤ 18 and between three and six carbon atoms in membered rings (as greater than six will be greater than the width of the MX_6 octahedra of the perovskite); (4) solubility is a prerequisite for solution processing; (5) hydrogen bonding alters the arrangement of spacers; and (6) reactivity in solution impacts the spacer you intend to use.

These rules also apply to 3D-to-2D conversion to form a 2D/3D heterostructure, meaning that butylammonium can form a 2D passivation layer, whereas tetramethylammonium cannot. However, various examples exist, suggesting that the formation dynamics are more complex in 3D-to-2D conversion. For instance, phenethylammonium², pyrene-methylammonium⁹, pyrene-ethylammonium⁹, octyldiammonium¹⁰ and octylammonium¹¹ can all form 2D perovskite single crystals but have been observed not to induce conversion from 3D to 2D perovskite under certain circumstances. Thus, indirect formation of 2D/3D heterostructures requires an expansion of the factors identified by Kanatzidis and colleagues.

Confirming the non-existence of a 2D phase is non-trivial as evidence from one technique may be disproven by another. For example, X-ray diffraction (XRD) is often used to distinguish 2D from 3D perovskites as the crystal structure of 2D perovskite is elongated compared with its 3D counterpart. However, Caiazzo et al.¹² found that films treated with a 1 mg ml^{-1} solution of 2H-benzotriazol-2-ylethylammonium iodide in isopropanol (IPA) showed no obvious

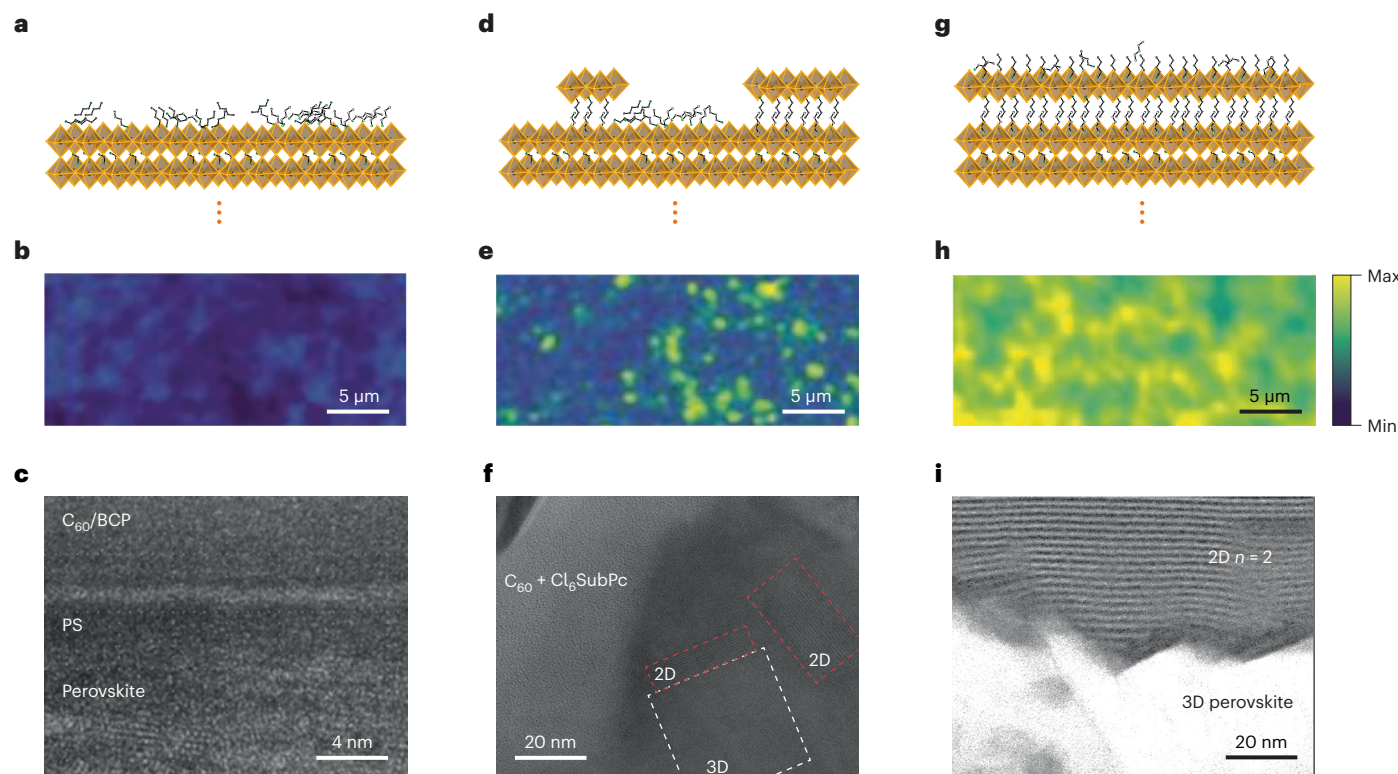


Fig. 3 | Three possible outcomes of applying ammonium ligands on top of perovskite films through solution processing. **a–i**, Illustrations (**a**, **d** and **g**), hyperspectral images of ~600 nm photoluminescence emission (**b**, **e** and **h**) and transmission electron microscopy (TEM) images (**c**, **f** and **i**) of passivating ligands not intercalating with perovskite and no conversion from 3D to 2D perovskite (**a**–**c**), a non-conformal 2D passivation layer where 2D perovskite is not present across the entire film surface (**d**–**f**) and a conformal 2D/3D heterostructure (**g**–**i**). **a**, Passivating cations atop 3D perovskite. Note that this layer itself may not be conformal. **b**, A perovskite surface without a 2D passivation layer. **c**, A PSC stack using an ultra-thin layer of molecular passivant polystyrene (PS).

d, A 3D perovskite surface partially transformed into 2D perovskite. **e**, A 3D perovskite surface below a non-conformal 2D passivation layer. **f**, A PSC stack with a non-conformal 2D passivation layer (indicated by a red dashed box) over a 3D perovskite layer (indicated by a white dashed box). **g**, A 3D perovskite surface conformally coated by 2D perovskite. **h**, A perovskite surface with what appears to be a conformal 2D passivation layer. **i**, A PSC stack with what appears to be a conformal 2D passivation layer. Max, maximum; Min, minimum. Panels adapted with permission from: **b**, **e**, **h**, ref. 6, Elsevier; **c**, ref. 49, Wiley; **f**, ref. 142, Elsevier; **i**, ref. 41, AAAS.

2D structural peaks on XRD, but photoluminescence associated with 2D perovskite was visible¹². Thus, we can only provide a sensible list of properties that (in addition to the rules from Kanatzidis and coworkers) influence 2D/3D formation when using an indirect deposition method. These are summarized in Fig. 4 and include: the concentration of ligand in solution; temperature; solvent polarity; 3D perovskite composition; anion steric hindrance; and the reactivity between 2D and 3D cations. Definitive studies comparing different ligands in all possible variations do not exist. Still, a summary and discussion of these parameters is provided below.

Concentration of ligand in solution

For 2D perovskites to form, the concentration of large cations must be high enough to intercalate and produce a coherent structure. Various studies compare ligand concentration with 2D perovskite formation using XRD, photoluminescence and absorption measurements^{12,13}, but—as mentioned above—it is difficult to make definitive statements based on these data. A comprehensive study was undertaken by Lai et al.¹⁴ who washed $\text{Cs}_{0.12}\text{FA}_{0.8}\text{MA}_{0.08}\text{PbI}_{1.8}\text{Br}_{1.2}$ films with different concentrations of 2-thiophene ethylammonium chloride (TEACl) in IPA. XRD results showed a 2D phase only for films washed with $>1 \text{ mg ml}^{-1}$ solutions of TEACl. Using X-ray photoelectron spectroscopy (XPS), they found that the A site/Pb ratio only exceeded 1 for TEACl concentrations $\geq 1 \text{ mg ml}^{-1}$. As this is necessary in the formation of TEA_2PbI_4 , it suggests that the 0.5 mg ml^{-1} wash resulted in one of the scenarios depicted in

Fig. 3a,d: either no 2D perovskite formation or only partial coverage. For $>1 \text{ mg ml}^{-1}$ TEACl concentrations, either scenario from Fig. 3d,g is the result: partial or conformal 2D coverage.

Degani et al.¹⁵ used sputtering XPS to determine whether or not a 2D passivation layer had formed. They washed $\text{Cs}_{0.05}(\text{FA}_{5/6}\text{MA}_{1/6})_{0.95}\text{Pb}(\text{I}_{0.85}\text{Br}_{0.15})_3$ films with a low-concentration solution of 4-chloro-phenylethylammonium iodide (Cl-PEAI) (2 mM in CB:IPA (9:1)) and annealed the films at 100°C for 30 min. The chloride signal in XPS from Cl-PEAI disappeared after etching only 0.5 nm into the film surface. As XPS is highly surface sensitive (~2 nm penetration depth) and one unit cell of PEA_2PbI_4 is ~1.7 nm, the researchers concluded that using a low enough concentration of ligand (even one that can in principle form a 2D perovskite) will result in the formation of a passivation layer atop 3D perovskite without the formation of any 2D structure. Hyperspectral images from these films suggest that they are uniformly passivated, although as the passivation layer is so thin it is difficult to determine conformativity¹⁶.

Temperature

As previously mentioned, after washing a perovskite film with a 2D-forming ligand solution, the formation of 2D perovskite may be induced by heating. The foremost example of this came from Jiang et al.², who showed that surface PbI_2 reacts with PEAI to form PEA_2PbI_4 upon heating. Similar results have been seen for 3-(trifluoromethyl) phenethylammonium iodide (CF₃-PEAI)¹⁷. Additionally,

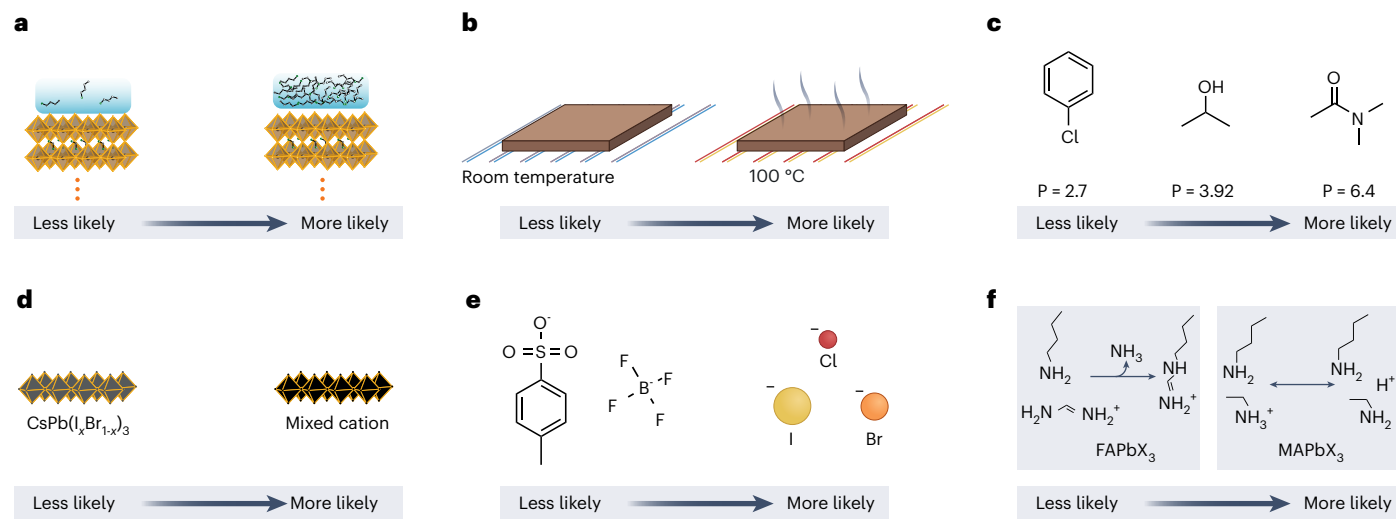


Fig. 4 | Factors driving the formation of a 2D perovskite on top of 3D perovskite. **a–f**, Six factors that drive the formation of 2D perovskite on top of 3D perovskite include solution concentration (**a**) temperature (**b**), solvent polarity (**c**), perovskite composition (**d**), anion steric hindrance (**e**) and amine reactions (**f**). **a**, Higher concentrations of cation in solution increase the chances of 2D formation. **b**, Annealing films after cation deposition can lead to the growth of a 2D layer. **c**, Dissolving cations in polar solvents can dissolve more of the 3D perovskite surface, leading to 2D perovskite formation. **P**, polarity index. **d**, All-inorganic perovskites are more resistive to forming 2D perovskite from

ammonium cation deposition, probably to due to stronger ionic bonds in the 3D perovskite. **e**, It has been shown that using large organic anions tends to inhibit the conversion of 3D to 2D perovskite when solution processing. **f**, It is possible to convert from 3D to 2D perovskite using amines rather than ammonium salts. This occurs through protonation of MA in MA-based perovskite, which acts to displace MA, facilitating the conversion into 2D perovskite. In FA-based perovskite, amines tend to react directly with the FA molecule, which can produce molecules that form 2D perovskite or other species.

in situ XRD has shown that a similar conversion for *n*-hexyl trimethyl ammonium bromide occurs after annealing¹⁸. Kodalle et al.¹⁹ examined PEAI washing using *in situ* photoluminescence measurements. They found that some 2D perovskite is produced immediately upon deposition of PEAI, but more is formed during annealing.

Interestingly, long-term annealing studies from Park²⁰ and Chakkalamalayath²¹ show that PEAI-passivated films lose diffraction and emission from 2D perovskite when annealed for over 1 h, suggesting that the 2D passivation layer is less stable than usually considered^{22,23}. This is discussed further in the stability section.

Solvent polarity

Using a solvent with high polarity, such as IPA or dimethylformamide dissolves some of the underlying perovskite when washing the film. This can result in favoured formation of quasi-2D perovskite over purely 2D perovskite²⁴. Using high concentrations of ligand salt in IPA results in crystallization of 2D perovskite from PbI_2 to form 2D platelets on the film surface. Mixing in non-polar solvents results in slower crystallization via ligand intercalation and gradual dimensional reduction⁵. Studies by Bawendi, Hagfeldt and colleagues^{22,23} suggest that when using purely non-polar solvents such as chloroform the formation of 2D perovskite is dependent on the presence of PbI_2 at the surface. A lack of PbI_2 inhibits the formation of 2D perovskite, leaving more unreacted ammonium salt^{22,23}.

3D perovskite composition

The A-site bond strength is higher in perovskites using inorganic caesium at the A site compared with formamidinium (FA) or methyl-ammonium (MA), making all-inorganic cells thermally stable at temperatures above 100 °C²⁵, whereas FA cells are stable below 95 °C²⁶ and MA-based cells are stable below 60 °C²⁷. Logically, one would expect resistance to 2D ligand ingress to follow the same pattern, and evidence exists to support this. For example, Li et al.²⁸ found that even after washing $\text{CsPb}(\text{I}_x\text{Br}_{1-x})_3$ films with extremely high concentrations of PEAI in IPA (100 mM), no 2D perovskite formation occurred. 2D formation did occur on a CsPbI_3 film after washing with a 12 mM

solution of phenylbutylammonium iodide in IPA:CB (1:4), suggesting that the less stable structure of CsPbI_3 compared with $\text{CsPb}(\text{I}_x\text{Br}_{1-x})_3$ may allow for ligand intercalation²⁹. Additionally, Proppe et al.⁵ observed that when MAPbI_3 undergoes conversion from 3D to 2D, it occurs via intercalation with PbI_2 sheets, whereas using FA-based 3D perovskite, larger slabs of 3D perovskite are broken down via gradual dimensional reduction, suggesting that MA is more easily displaced than FA in the reaction process.

Anion steric hindrance

The factors identified by Kanatzidis and colleagues tell us that increased steric hindrance around the ligand ammonium group reduces the propensity for 2D perovskite to form. A recent report from Tan et al.¹¹ suggests that the steric hindrance of the salt anion may also play a role. They found that after washing (FAPbI_3)_{0.95}(MAPbBr_3)_{0.05} films with 10 mM solutions of octylammonium-X in IPA, 2D perovskite was only formed for X = I or Br and not for X = BF_4^- or tosylate. Interestingly, they correlate this lack of 2D formation with increased device stability. 2D-forming salt solutions induced a negative work function shift, which they suggest can promote ion migration and decrease stability.

Reactivity between 2D and 3D cations

Although this factor is among those identified by Kanatzidis and colleagues, it is worth noting that chemical reactions can take place between organic species during solution deposition, and these can influence the formation of 2D perovskite or molecular cation passivation layers. When using amine (rather than ammonium) solutions, ligands react quickly to deprotonate MA⁺ cations in MAPbI_3 , with the formation of PbI_2 and reversible reactions forming Pb-iodo-amine/amide complexes³⁰. This does not occur in FA-based perovskite as amines tend to react directly with the FA molecule rather than forming coordinate compounds with Pb^{31,32}. Both of these processes impact 2D formation, as deprotonation of MA⁺ produces PbI_2 to form 2D perovskite when using an MA-based composition, and molecules that cannot form 2D perovskite may form from reactions with FA-based perovskites.

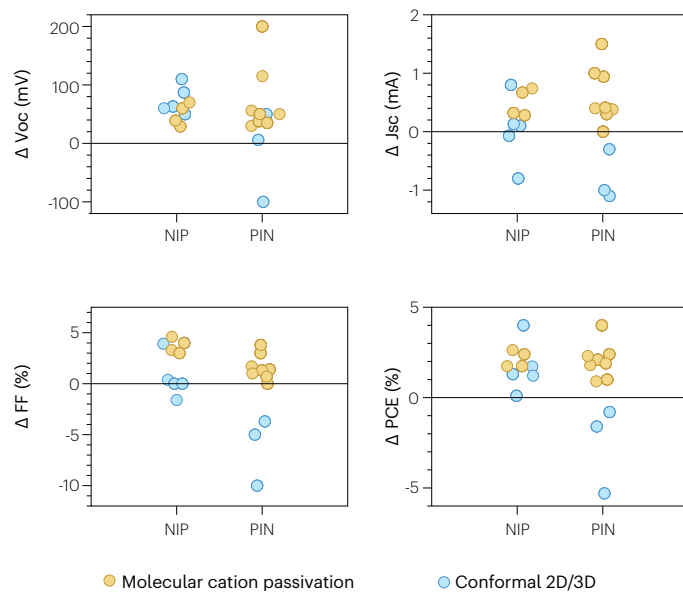


Fig. 5 | Impact of molecular or 2D perovskite passivation layers on solar cell performance.

Here, ΔX represents the difference in X between control and passivated devices in each study. An average between device batches was used if provided. Device statistics were taken from 50 studies using ammonium cation or 2D surface treatments. More details are provided in Source Data Fig. 5. Of these, eight used a conformal 2D passivation layer (conformal 2D/3D)^{3,4,40,41,65,75,143,144} and 12 used an ammonium cation without the formation of 2D perovskite (molecular cation passivation)^{15,16,20,28,32,42,43,115,145–148}. FF, fill factor.

Implications for photovoltaic efficiency

There are two standard architectures for PSCs: those fabricated in the negative–intrinsic–positive (n–i–p) configuration, in which a hole transport layer is deposited onto the top perovskite surface, and those fabricated in the p–i–n configuration, in which an electron transport layer (ETL) is deposited onto the top perovskite surface. Comparing results from these two architectures is useful to determine how passivation layers facilitate or inhibit hole or electron transport.

Although many papers use fabrication methods, which produce 2D perovskite atop a 3D film, few give conclusive evidence of the conformality of the 2D passivation layer. This is important as to understand the results from these studies we must disambiguate between conformal 2D layers, non-conformal 2D layers, and molecular cation passivation layers. We assessed the results from 50 articles that use ammonium ligand passivation and attempt to characterize the passivation layer, and categorized them as either: (1) molecular cation passivation (information on the conformality of these layers is scarce); (2) no 2D perovskite detected (when an ammonium cation treatment that could form 2D perovskite is used but no decisive evidence is shown to confirm the presence of a 2D structure); (3) 2D perovskite detected (but without conclusive data around its coverage); and (4) conformal 2D/3D heterostructure. Details on the studies taken into consideration are provided in Source Data Fig. 5. To remove ambiguity, we compare devices from groups (1) and (4) only in Fig. 5. The open-circuit voltage (V_{oc}) of passivated devices was improved by passivation in the majority of reports, which is to be expected. The fill factor was also usually improved, which is reasonable as fill factor tends to increase with increasing V_{oc} . Comparing n–i–p with p–i–n devices, we found that conformal 2D/3D bilayer passivation and molecular cation passivation have a similar effect on n–i–p devices. In contrast, for p–i–n cells, there is a distinct difference in performance, with conformal 2D/3D films performing poorly due to decreases in the current and fill factor. To explain these differences, we must consider how passivation affects

surface defects, interfacial trap states and band alignment between perovskite and transport layers.

Surface defects

One might reasonably wonder why ammonium ligands passivate so effectively. One suggestion comes from density functional theory calculations³³. Considering possible defects, FA interstitials and I interstitials have the lowest formation energies, producing trap states within the bandgap. Passivation calculations indicate that ammonium ligands are so effective as they remove A-site vacancies easily (Fig. 6a) and hydrogen bond to remove interstitial defects (Fig. 6b)³⁴. Additionally strong surface binding and the bulky nature of 2D cations may act to stabilize these defect sites.

Without passivation, defects within the bandgap induce non-radiative recombination, thus an obvious indication that a passivation strategy is healing defects is the detection of films with higher photoluminescent quantum yields (PLQYs). The maximum V_{oc} extractable from a solar cell is equal to the quasi-fermi level splitting (QFLS) in the absorber layer. This is related to the PLQY via the Ross relation³⁵

$$\text{QFLS} = k_B T \ln(\text{PLQY}) + \text{QFLS}_{\text{rad}},$$

where k_B is Boltzmann's constant, T is temperature and QFLS_{rad} is the QFLS for the material with no non-radiative recombination. From this, we find that a doubling in PLQY increases QFLS by ~18 meV (and thus the maximum V_{oc} by ~18 mV), and increasing PLQY by an order of magnitude increases the maximum V_{oc} by ~60 mV. As shown in Fig. 5, many papers claim that V_{oc} increases around or above 60 mV. If defect healing on the perovskite surface is the sole cause of this V_{oc} increase, one would expect huge increases in PLQY for neat perovskite films after passivation. Among the data from literature we surveyed (Source Data Fig. 5), 13 papers report PLQY or QFLS values and these consistently show that QFLS is increased by passivation (as one would expect). However, the QFLS difference between control and passivated films is consistently smaller than the recorded V_{oc} difference in devices (Fig. 6c). This suggests that although healing perovskite surface defects does contribute to increasing V_{oc} other factors should also be considered.

Interfacial traps

Beyond defects in each of the individual semiconductor layers of the solar cell stack, it is known that non-radiative recombination is much higher at charge transport layer (CTL)/perovskite interfaces^{36,37}. PLQY is generally quenched by one to two orders of magnitude using a C₆₀ ETL (for example, ref. 37). From Fig. 6c, the differences in QFLS and V_{oc} after passivation (ΔQFLS and ΔV_{oc}) are roughly equal for films connected to CTLs, suggesting that a decrease in both surface and interfacial defects explains why ammonium ligand passivation is so beneficial.

To understand why either molecular cation passivation or 2D perovskite passivation can inhibit interfacial trap states, we must consider what causes interfacial recombination. Although this is still a subject of research, this phenomenon is usually attributed to cross-interface recombination (minority carriers in the perovskite to majority carriers in the CTL) or the introduction of mid-bandgap interfacial states (Fig. 6d)^{28,36–38}. Researchers prevent recombination via mid-gap interface states by physically separating the perovskite and CTLs (Fig. 6e)³⁹. All of the methods described herein should produce either full or partial separation of perovskite and CTLs to inhibit this. Cross-interface recombination is suppressed by decreasing the minority carrier population in the perovskite near the interface. To achieve this, energetic alignment at the interface must be modulated (Fig. 6f).

Energetic alignment

Band alignment measurements from films with conformal 2D passivation layers show that these 2D layers tend to align to block electrons

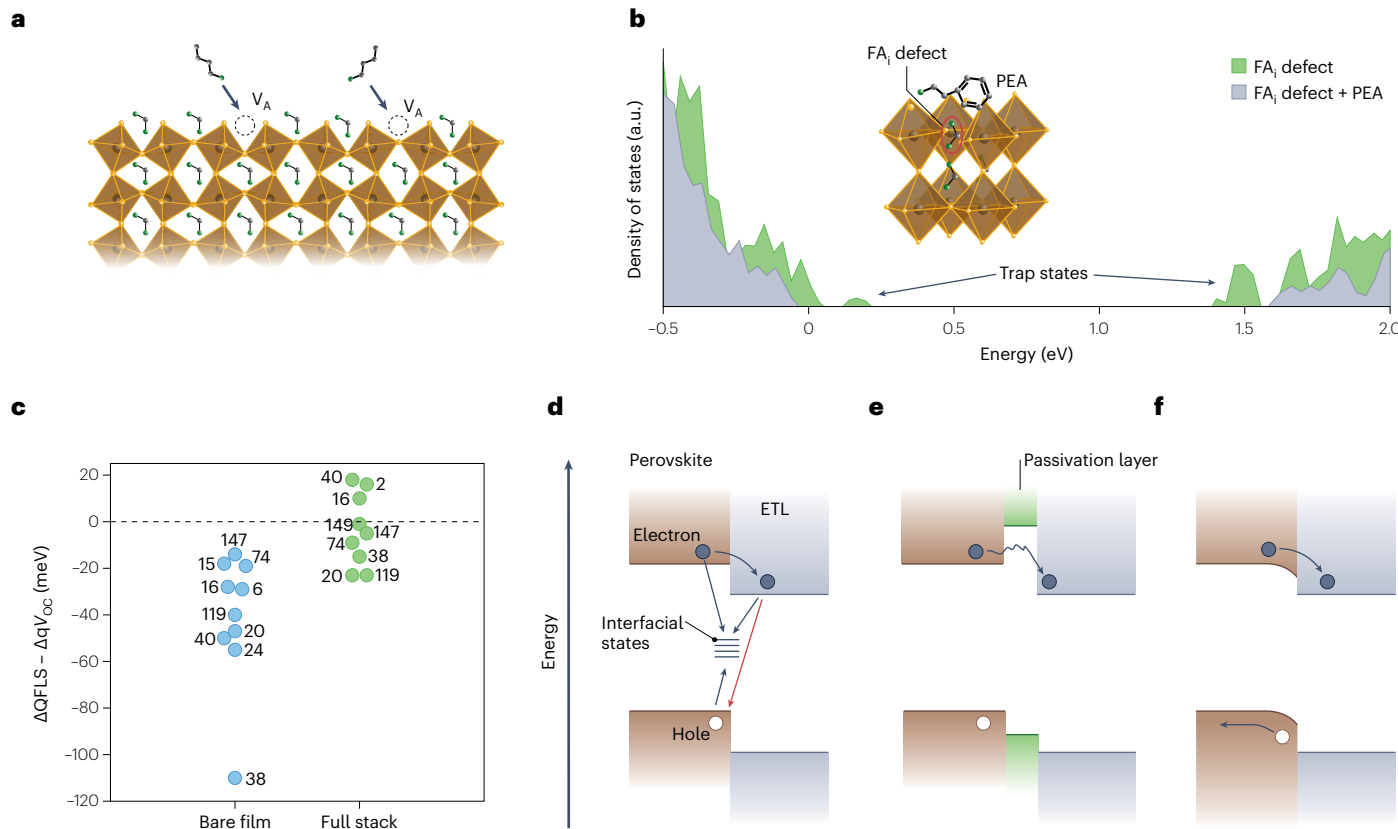


Fig. 6 | Passivation mechanisms. **a**, Schematic of ammonium ligands passivating A-site vacancies, V_A . **b**, Results from density functional theory energy band calculations for an FA interstitial defect (FA_i) with and without a benzene-based passivating molecule. The trap states before introducing the benzene molecule to the surface are highlighted by arrows. **c**, Difference between $\Delta QFLS$ and ΔqV_{oc} for perovskite films and devices, where q is the elemental charge^{2,6,15,16,20,24,38,40,74,119,147,149}. The numbers represent reference citations. Details are reported in Source Data Fig. 5. Here, ΔX represents the difference in X between control and passivated films. QFLS values were calculated from PLQY

measurements of either bare films or films attached to CTls. **d**, Schematic of commonly cited sources of interfacial recombination. The green arrows represent recombination at interfacial traps states and the red arrow represents cross-interfacial recombination. **e**, Band structure with a passivator that physically separates the perovskite and ETL. **f**, Band structure with a passivator that reduces the minority carrier population at the perovskite/ETL interface. Panels adapted with permission from: **a**, ref. 150, Springer Nature Limited; **b**, ref. 34, American Chemical Society.

and allow holes, and that they shift the perovskite surface to a higher vacuum level (Fig. 7a,b), all of which favour contact with a hole transport layer (as in n-i-p devices)^{3,4,40}. This probably explains the poor performance of p-i-n cells using conformal 2D passivation layers (Fig. 5). One method to decrease electron blocking is to use a quasi-2D perovskite passivation layer. Quasi-2D perovskites are repeating structures in which multiple units of 3D perovskite are confined by insulating cations (the number of 3D unit cells is defined by n). They typically have a deeper conduction band minimum than pure ($n = 1$) 2D perovskite (Fig. 7b). Chen et al.²⁴ and Azmi et al.⁴¹ used this concept to produce 2D passivated p-i-n devices with excellent fill factors (>82%); however, it is unclear whether a conformal 2D passivation layer was produced in either work. Indeed, when using a concentration that produced a conformal passivation layer in hyperspectral images ($\geq 1.5 \text{ mg ml}^{-1}$ oleylammmonium iodide in chloroform), Azmi et al. found that PCE decreased slightly. Sidhik et al. used acetonitrile to directly deposit quasi-2D perovskite without dissolving the 3D perovskite substrate. As a result of applying a 55-nm, conformal, $n = 3$, quasi-2D passivation layer to a p-i-n cell, its efficiency decreased by >5 absolute percentage points, suggesting that even quasi-2D passivation layers may be harmful in p-i-n cells.

Molecular cation passivation layers can also alter surface band alignment. Li et al.³⁸ suggest that this is mediated by dipole moment. CF3-PEA, for example, has a large dipole moment so it imparts strong charge separation across the perovskite/CTL interface, resulting in

perovskite surfaces with deeper band alignment that are more suited to an ETL (Fig. 7c). Using an ammonium ligand with a small dipole moment can result in the opposite, preferred alignment towards a hole transport layer^{28,42,43}. Filling vacancies and surface polishing can also alter surface states for improved alignment^{38,44}. This explains why molecular cation passivation methods can be effective in both n-i-p and p-i-n configurations.

Carrier extraction

Passivating agents generally form insulating layers that, if too thick, can impede charge extraction. However, if grown thin enough (~1 nm), carriers can traverse the layer without the introduction of substantial series resistance. This transport is generally ascribed to tunnelling, although it has been debated whether nanostructured cracks in the insulating layer play a critical role^{45,46}. Either way, thick (for example, >5 nm) passivating layers generally limit solar cell performance. For PSCs, many different passivation methods have been developed, most of which employ an extremely thin (around a few nanometres) layer of low conductivity passivant (LiF⁴⁷, MgF³⁹, PbSO₄⁴⁸, insulating polymer⁴⁹ and so on). Conversely, when using conformal 2D perovskite as a passivation layer, layer thicknesses of >50 nm have shown improved performance^{3,4}. This suggests that carriers are not traversing the 2D perovskite via tunnelling, but instead the 2D passivation layer is energetically aligned with the perovskite and conductive enough for transport.

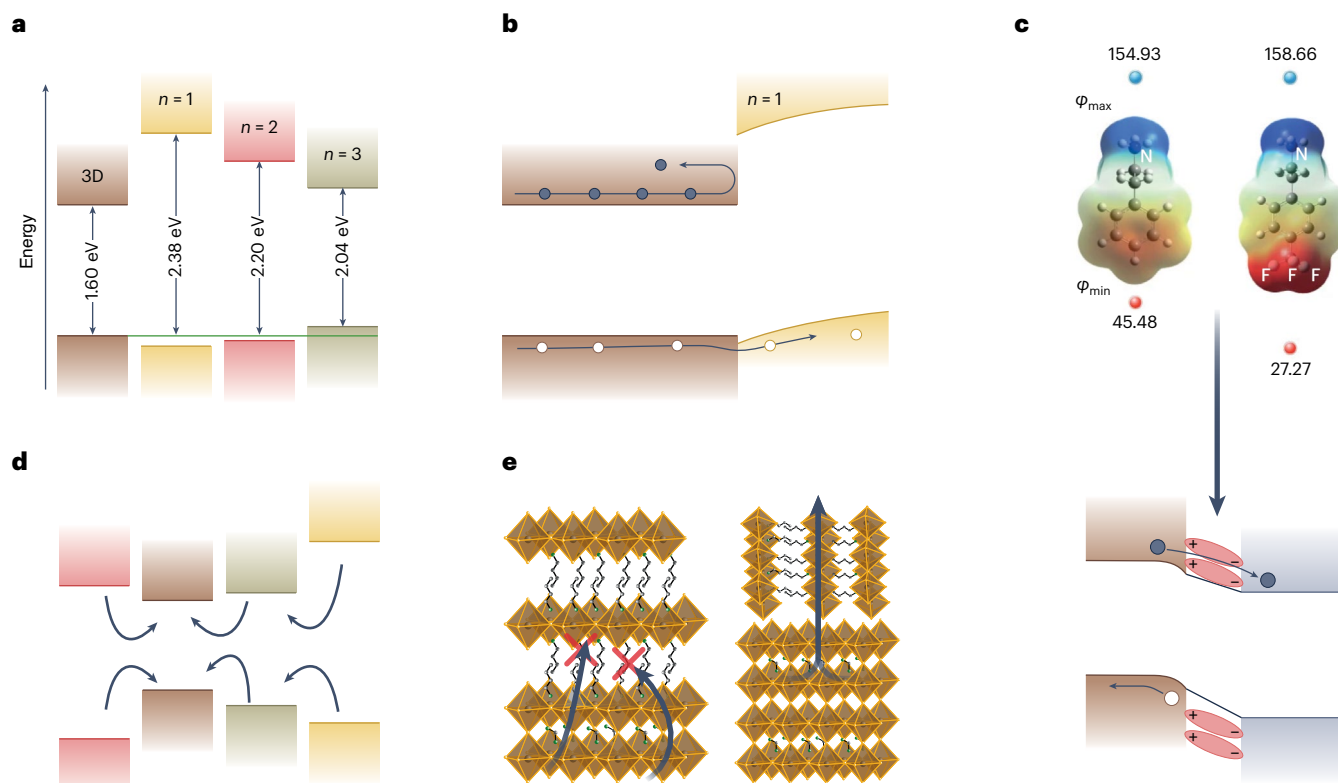


Fig. 7 | Photophysics of 2D perovskite passivation layers and molecular cation-passivated PSCs. **a**, Typical band structure of 3D perovskite compared with 2D and quasi-2D perovskite. The green line indicates the valence band maximum for 3D perovskite. **b**, The energetic alignment of 2D and 3D perovskite is such that the 2D passivation layer is aligned to block electrons (black dots) and accepts holes (white dots). **c**, Illustration of the dipole effect induced by a molecular cation passivation layer. Electrostatic potentials (ϕ) (ϕ_{\max} , blue; ϕ_{\min} , red) of PEA and $\text{CF}_3\text{-PEA}$ cations are shown. When placed between the perovskite (brown)/electron transport layer (blue) in a device, the electrostatic dipole

can induce positive band bending. **d**, Schematic of carrier trapping in mixed quasi-2D perovskite films with different band structures. If adjacent layers have lower n values (which have narrower bandgap energies), charges can be trapped, hindering charge transport. The trapping process is indicated by black arrows. **e**, Schematic of vertically and horizontally orientated 2D passivation layers atop 3D perovskite. The black arrows represent the direction of charge extraction. In films using horizontally orientated 2D perovskite, carrier extraction is inhibited. (a) is adapted from⁴; (c) is adapted from²⁸. Panel c adapted with permission from ref. 28, Springer Nature Limited.

Quantum confinement in 2D perovskite decreases mobility considerably, particularly for carriers moving between Pb halide units. Within quantum confined units, however, quasi-2D perovskite with $n \geq 3$ exhibits mobilities similar to 3D perovskite, thus vertically aligned quasi-2D perovskite films exhibit high current densities (Fig. 7e)⁵⁰. Unfortunately, most 2D passivation layers are reported to form horizontally stacked quantum wells that inhibit transport. Additionally, it is important to note that mixed dimensional phases in quasi-2D perovskite films induce charge trapping in low-n regions (that is, regions with a lower bandgap) within the film, which inhibits charge extraction (Fig. 7d)⁵¹. Thus, the ideal 2D passivation layer is a pure-phase, quasi-2D perovskite oriented vertically (for vertical charge transport in a device)⁵². Sidhik et al.⁴ report that direct deposition of $n = 3$ quasi-2D perovskite produces a pure-phase 2D perovskite passivation layer with mixed horizontal/vertical orientation, allowing diffusion over 100 nm. One can also remedy poor charge extraction by using non-conformal passivation (like that found in a passivated emitter rear contact cell)⁵³ or an ultra-thin cation passivation layer.

The results in Fig. 5 show that molecular cation passivation tends to increase fill factor and short-circuit current (J_{SC}), suggesting that this is an advantage over 2D passivation layers. Charge extraction in molecular cation passivation layers is influenced by the orbital arrangement of the molecules. This can result in more efficient extraction in molecularly passivated films²⁸.

An innovative method to overcome poor mobility in 2D passivation layers was developed by Zhu et al.⁵⁴. Using a chiral diammonium ligand

treatment (*N,N*-dimethyl-1,3-propane diammonium iodide in IPA), they produced 2D perovskite in a metastable structure that decreased quantum confinement, resulting in improved diffusion lengths in $n = 1$ pure 2D perovskite films. When used to passivate a 3D PSC, it is unclear whether their method produced a conformal 2D passivation layer on top of 3D perovskite, but it did result in improved performance against standard surface treatments (PEAI and butylammonium iodide), resulting in a maximum PCE of 24.7%.

Ion migration

Metal halide perovskites are both electronic and ionic conductors. High defect densities generate high ion densities (up to 10^{17} cm^{-3}) and provide pathways for ion migration⁵⁵. The migration energy of halides is lower than that of cation or metal species⁵⁶, meaning that halide drift is generally attributed to ionic conduction. In PSCs, the built-in electric field induces mobile ions to migrate to the interfaces. This results in a loss of current due to flattening bands at the device interface, or a buildup of insulating interface material⁵⁷. The current density of most perovskite cells is well below the optical limit⁵⁸. Indeed, significant photoluminescence has been observed in cells under short-circuit conditions, meaning that carriers are recombining without being extracted⁵⁹. There is a trend towards higher J_{SC} after passivation for most devices in Fig. 5. One explanation for this is lower defect (and thus ion) densities at the perovskite surface, meaning decreased ion screening. Several 2D perovskite and molecular cation passivation layers have been shown to impede ion migration in films^{25,38,60}.

Scalability

The majority of PSC research uses solution-based deposition by spin-coating thin films; however, this method is not scalable and methods such as blade coating, spray coating or evaporation are preferable at the industrial level. Using an indirect surface passivation method (converting the perovskite surface from 3D to 2D), the reaction time between 2D cations and 3D perovskite must be controlled very precisely, with many reports of dynamic spin-coating^{2,61}.

Considering this, upscaling using a solution-processed method will be difficult, so alternative approaches should be found. For instance, 3D to 2D conversion using scalable vapour deposition has been demonstrated on MAPbI₃ cells using butylamine vapour (room temperature)⁶² and vapourized butylammonium iodide (120 °C)⁶³. 2D passivation with this technique improved the stability of devices regardless of the method used, suggesting that vapour deposition is a valid alternative for scale-up. The PCE of cells was only increased by the room temperature technique, however, which is unsurprising as prolonged processing above 100 °C is detrimental for MAPbI₃ perovskites⁶⁴. Vacuum deposition has been demonstrated, but unfortunately without PCE improvement⁶⁵. Park et al.²⁰ demonstrated that the processing window for solution exposure is increased when using an ammonium cation that does not form 2D perovskite, meaning that solution processing may be feasible. To this end, Liu et al.⁴² demonstrated 26 cm² perovskite modules with >21% PCE by utilizing a non-2D-forming diammonium.

Implications for solar cell stability

2D perovskite and molecular cation passivation layers often result in improved stability under humid conditions due to the hydrophobic nature of the capping ligands^{3,41,66}. For commercial applications, moisture is less important than other stressors as cells are encapsulated, and encapsulated devices have demonstrated little to no degradation after 1 year of outdoor operation⁶⁷. More detrimental to performance are illumination and temperature. Both stressors contribute to ion migration, which screens the built-in electric field, causes irreversible degradation of the perovskite layer and decreases electrode conductivity⁶⁸. To prevent this, researchers have inserted barrier layers (indium oxide⁶⁹, SnO₂⁷⁰ and Cr⁷¹), which hinder halide migration. 2D perovskite is known for its lower susceptibility to ion migration than 3D perovskite⁷², and has been shown to decrease ion loss in operating cells⁷³. Studies testing molecular cation-passivated perovskite have found similar results¹¹ and passivated cells produce longer operating lifetimes compared with unpassivated cells.

To estimate the extent to which passivation extends lifetime, we analysed stability results reported in the literature for encapsulated cells (or those tested under an inert atmosphere) under constant illumination. As each study used a different temperature, we used the Arrhenius factor model from ref. ⁶⁸ to equilibrate each measurement to 35 °C. In Fig. 8, we show that non-passivated devices generally exhibit lifetimes of around one month. After passivation, lifetimes typically extend to several months, and in five cases we estimate multiple-year lifetimes^{4,25,74,75}. Passivation improves lifetime by between two and 20 times. However, as more emphasis is usually put on demonstrating improved stability compared with controls, this effect may be overestimated. Note that it is unclear whether the films from the 2D detected category contained a conformal or non-conformal 2D perovskite passivation layer, but all of the results are included for completeness.

Despite impressive results, recent studies have questioned the stability of 2D passivation layers in PSCs. Sutanto et al.⁷⁶ demonstrated that over time 2D perovskite can degrade from pure 2D $n = 1$ to $n \geq 2$ quasi-2D perovskite, suggesting that ligands continue to penetrate and bisect 3D perovskite units after 2D perovskite crystallization. Devices passivated with ligands that converted more quickly from pure 2D to quasi-2D perovskite showed worse stability under illumination⁷⁶. Using

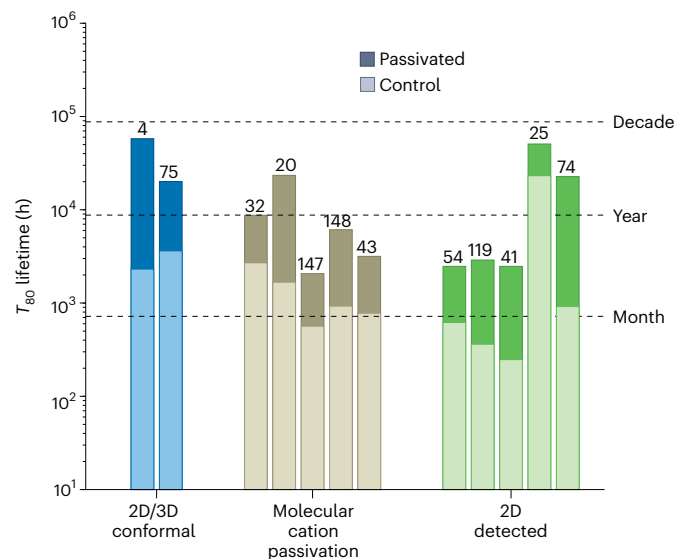


Fig. 8 | Estimated T_{80} lifetimes extrapolated from stability data in literature reports. Only stability data for encapsulated devices (or those tested under an inert atmosphere) under continuous illumination are shown here (full details of the solar cell parameters are reported in Source Data Fig. 5). The numbers represent reference citations. 2D/3D conformal refers to studies demonstrating the use of a conformal 2D passivation layer^{4,75}. Molecular cation passivation refers to those showing conclusive evidence that 2D perovskite was not formed^{20,32,43,147,148}. 2D detected refers to studies in which 2D perovskite was shown to exist on the perovskite surface, but it was either non-conformal or the conformality of the layer was unknown^{10,25,54,74,119}. The T_{80} lifetime was estimated using the Arrhenius model used in ref. ⁶⁸.

a lower-concentration ammonium ligand treatment (10 mM compared with 60 mM), Kamat and coworkers²¹ showed that when stressed with illumination and heat, the amount of 2D perovskite present on a film surface decreased over time. Correlating the results at different temperatures, the activation energy for PEA ion migration was calculated to be 36.6 kJ mol⁻¹—less than half that previously calculated by Kamat's team for halide migration in bulk 2D perovskite films⁷⁷. Park et al.²⁰ saw similar results to those of Kamat's team and used time-of-flight secondary ion mass spectrometry to confirm that PEA ligands move from the surface towards the bulk of the perovskite. Correlating this with PLQY, they found that PEA-treated films had similar 85 °C stability to a film with no passivation. To avoid losing passivating cations from the perovskite surface, they used anilinium as it cannot produce 2D perovskite and thus cannot readily bisect the perovskite crystal structure. Adding three fluorine atoms to the anilinium molecule increased the strength of binding with the perovskite surface, resulting in improved efficiency (up to 24% PCE for 1.55 eV perovskite) and stability (our estimate is a T_{80} (the time required for the cell performance to degrade to 80% of its initial value) of -2 years at 1 sun and 35 °C; Fig. 8)²⁰.

Wang et al.⁷⁸ note that the pKa value of most ammonium cation treatments is low relative to that of FA; thus, these cations are more likely to deprotonate, leading to structural degradation and reactions with FA forming ammonia, which can dissolve perovskite. Using (phenethylamino) methaniminium—a cation similar to PEA but with a larger pKa value—to passivate cells improved lifetimes twofold (we estimate a T_{80} of ~3 years at 1 sun and 35 °C).

It is worth highlighting that all-inorganic 2D perovskite (Cs₂PbI₂Cl₄) can be formed by washing a CsPbI₃ film with a CsCl solution. Zhao et al.²⁵ used this approach, along with several other barrier layers, to produce -1.7 eV PSCs with 17% PCE and a T_{80} lifetime of 2,100 h at 110 °C (estimated to be a T_{80} of -5 years at 35 °C). The study

contained no direct evidence of 2D passivation layer conformality or longevity; however, one might expect all-inorganic 2D passivation layers to be more stable than their hybrid counterparts. The 2D treatment decreased the activation energy for ion migration from 0.29–0.53 eV and increased lifetimes twofold (Fig. 8).

The approach reported by Sidhik et al.⁴ with the direct deposition of a conformal 2D perovskite onto a $\text{Cs}_{0.05}(\text{MA}_{0.10}\text{FA}_{0.85})\text{Pb}(\text{I}_{0.90}\text{Br}_{0.10})_3$ film led to a notable improvement in stability. Using no other barrier layers, their 24.5% PCE n-i-p cells recorded a T_{90} of 2,000 h, whereas their control (21% PCE) dropped to 75% of its original efficiency after only 1,000 h. Interestingly, they also fabricated a cell using a butylammonium iodide treatment in IPA for indirect 2D-to-3D conversion. This cell recorded a T_{90} of 1,000 h, considerably worse than the direct 2D deposition film. The reduced stability could have been due to a lack of conformality, meaning that not all of the film surface was protected, or due to similar degradation to that mentioned in the paragraph above, indicating that directly deposited 2D passivation layers may be less susceptible to penetration into bulk perovskite.

Conclusion and outlook

Whether a passivation technique produces a conformal layer of 2D perovskite, a mixed 2D/organic layer or a non-conformal passivation layer will have an impact on the photophysics and stability of devices. It is difficult, for example, for conformal 2D passivation layers to be used to passivate n-type contacts, and non-conformal passivation layers may insufficiently suppress ion drift. However, recent results are encouraging and indicate that, if engineered properly, either molecular passivation layers with low penetration and high binding strength or 2D passivation layers with high stability can improve both the efficiency and stability of solar cells.

Deeper understanding of the stability of directly deposited 2D passivation layers is needed. If these passivation layers are more stable because their cations do not ingress into the 3D perovskite, then fabricating 2D passivation layers using bulkier cations than butylammonium may decrease this propensity even more, resulting in even longer lifetimes. Considering efficiency, it may be possible to increase carrier extraction further by depositing a vertically oriented $n \geq 3$ 2D passivation layer directly; however, this may not afford the same protection to ion diffusion as the protective spacers will not be aligned to block ion movement out of the cell.

Aiming to protect the 3D active layer, conformal 2D passivation layers have the advantage of protecting the entire film surface. Molecular cation passivation can theoretically result in a conformal monolayer that protects from ion diffusion without hindering charge transport, but this is difficult to achieve via solution processing. However, if a ligand can be engineered to anchor strongly to the perovskite surface, additional ligands can be washed from the surface without removing the first layer and this could be achieved. It remains to be seen whether a thin molecular passivation layer can afford the same protection as a thicker 2D passivation layer. However, the solar cell lifetime estimates in Fig. 8 show that using a molecular cation passivation layer or a conformal 2D passivation layer can afford stability beyond 2 years under 1 sun, suggesting that with further progress either passivation layer may ultimately provide enough protection to reach commercially acceptable durability (≥ 25 years).

References

- Chen, H. et al. Improved charge extraction in inverted perovskite solar cells with dual-site-binding ligands. *Science* **384**, 189–193 (2024).
- Jiang, Q. et al. Surface passivation of perovskite film for efficient solar cells. *Nat. Photon.* **13**, 460–466 (2019).
- Jang, Y. W. et al. Intact 2D/3D halide junction perovskite solar cells via solid-phase in-plane growth. *Nat. Energy* **6**, 63–71 (2021).
- Sidhik, S. et al. Deterministic fabrication of 3D/2D perovskite bilayer stacks for durable and efficient solar cells. *Science* **377**, 1425–1430 (2022).
- Proppe, A. H. et al. Multication perovskite 2D/3D interfaces form via progressive dimensional reduction. *Nat. Commun.* **12**, 3472 (2021).
- Ugur, E. et al. Front-contact passivation through 2D/3D perovskite heterojunctions enables efficient bifacial perovskite/silicon tandem solar cells. *Mater.* **6**, 2919–2934 (2023).
- Quan, L. N. et al. Ligand-stabilized reduced-dimensionality perovskites. *J. Am. Chem. Soc.* **138**, 2649–2655 (2016).
- Li, X., Hoffman, J. M. & Kanatzidis, M. G. The 2D halide perovskite rulebook: how the spacer influences everything from the structure to optoelectronic device efficiency. *Chem. Rev.* **121**, 2230–2291 (2021).
- Xue, J. et al. Reconfiguring the band-edge states of photovoltaic perovskites by conjugated organic cations. *Science* **371**, 636–640 (2021).
- Zhao, T., Chueh, C.-C., Chen, Q., Rajagopal, A. & Jen, A. K.-Y. Defect passivation of organic–inorganic hybrid perovskites by diammonium iodide toward high-performance photovoltaic devices. *ACS Energy Lett.* **1**, 757–763 (2016).
- Tan, S. et al. Stability-limiting heterointerfaces of perovskite photovoltaics. *Nature* **605**, 268–273 (2022).
- Ciaiazzo, A. et al. 3D perovskite passivation with a benzotriazole-based 2D interlayer for high-efficiency solar cells. *ACS Appl. Energy Mater.* **6**, 3933–3943 (2023).
- Gharibzadeh, S. et al. Record open-circuit voltage wide-bandgap perovskite solar cells utilizing 2D/3D perovskite heterostructure. *Adv. Energy Mater.* **9**, 1803699 (2019).
- Lai, H. et al. High-performance flexible all-perovskite tandem solar cells with reduced V_{oc} -deficit in wide-bandgap subcell. *Adv. Energy Mater.* **12**, 2202438 (2022).
- Degani, M. et al. 23.7% Efficient inverted perovskite solar cells by dual interfacial modification. *Sci. Adv.* **7**, 7930 (2021).
- Cacovich, S. et al. Imaging and quantifying non-radiative losses at 23% efficient inverted perovskite solar cells interfaces. *Nat. Commun.* **13**, 2868 (2022).
- Xia, J. et al. Deep surface passivation for efficient and hydrophobic perovskite solar cells. *J. Mater. Chem. A Mater.* **9**, 2919–2927 (2021).
- Hu, H. et al. Perovskite quantum wells formation mechanism for stable efficient perovskite photovoltaics—a real-time phase-transition study. *Adv. Mater.* **33**, 2006238 (2021).
- Kodalle, T. et al. Revealing the transient formation dynamics and optoelectronic properties of 2D Ruddlesden–Popper phases on 3D perovskites. *Adv. Energy Mater.* **13**, 2201490 (2023).
- Park, S. M. et al. Engineering ligand reactivity enables high-temperature operation of stable perovskite solar cells. *Science* **381**, 209–215 (2023).
- Chakkalamalayath, J., Hiott, N. & Kamat, P. V. How stable is the 2D/3D interface of metal halide perovskite under light and heat? *ACS Energy Lett.* **8**, 169–171 (2023).
- Yoo, J. J. et al. An interface stabilized perovskite solar cell with high stabilized efficiency and low voltage loss. *Energy Environ. Sci.* **12**, 2192–2199 (2019).
- Suo, J. et al. Interfacial engineering from material to solvent: a mechanistic understanding on stabilizing α -formamidinium lead triiodide perovskite photovoltaics. *Nano Energy* **94**, 106924 (2022).
- Chen, H. et al. Quantum-size-tuned heterostructures enable efficient and stable inverted perovskite solar cells. *Nat. Photon.* **16**, 352–358 (2022).
- Zhao, X. et al. Accelerated aging of all-inorganic, interface-stabilized perovskite solar cells. *Science* **377**, 307–310 (2022).

26. Juarez-Perez, E. J., Ono, L. K. & Qi, Y. Thermal degradation of formamidinium based lead halide perovskites into *sym*-triazine and hydrogen cyanide observed by coupled thermogravimetry-mass spectrometry analysis. *J. Mater. Chem. A Mater.* **7**, 16912–16919 (2019).
27. Brunetti, B., Cavallo, C., Ciccioli, A., Gigli, G. & Latini, A. On the thermal and thermodynamic (in)stability of methylammonium lead halide perovskites. *Sci. Rep.* **6**, 31896 (2016).
28. Li, T. et al. Inorganic wide-bandgap perovskite subcells with dipole bridge for all-perovskite tandems. *Nat. Energy* **8**, 610–620 (2023).
29. Steele, J. A. et al. Thermal unequilibrium of strained black CsPb₃ thin films. *Science* **365**, 679–684 (2019).
30. Kerner, R. A. et al. Amine additive reactions induced by the soft Lewis acidity of Pb²⁺ in halide perovskites. Part I: evidence for Pb-alkylamide formation. *J. Mater. Chem. C Mater.* **7**, 5251–5259 (2019).
31. Li, Z. et al. Ammonia for post-healing of formamidinium-based perovskite films. *Nat. Commun.* **13**, 4417 (2022).
32. Jiang, Q. et al. Surface reaction for efficient and stable inverted perovskite solar cells. *Nature* **611**, 278–283 (2022).
33. Yin, W.-J. et al. Unique properties of halide perovskites as possible origins of the superior solar cell performance. *Adv. Mater.* **26**, 4653–4658 (2014).
34. Oner, S. M. et al. Surface defect formation and passivation in formamidinium lead triiodide (FAPbI₃) perovskite solar cell absorbers. *J. Phys. Chem. Lett.* **13**, 324–330 (2022).
35. Ross, R. T. Some thermodynamics of photochemical systems. *J. Chem. Phys.* **46**, 4590–4593 (1967).
36. Stolterfoht, M. et al. The impact of energy alignment and interfacial recombination on the internal and external open-circuit voltage of perovskite solar cells. *Energy Environ. Sci.* **12**, 2778–2788 (2019).
37. Warby, J. et al. Understanding performance limiting interfacial recombination in pin perovskite solar cells. *Adv. Energy Mater.* **12**, 2103567 (2022).
38. Chen, H. et al. Regulating surface potential maximizes voltage in all-perovskite tandems. *Nature* **613**, 676–681 (2022).
39. Liu, J. et al. Efficient and stable perovskite–silicon tandem solar cells through contact displacement by MgFx. *Science* **377**, 302–306 (2022).
40. Sutanto, A. A. et al. 2D/3D perovskite engineering eliminates interfacial recombination losses in hybrid perovskite solar cells. *Chem* **7**, 1903–1916 (2021).
41. Azmi, R. et al. Damp heat-stable perovskite solar cells with tailored-dimensionality 2D/3D heterojunctions. *Science* **376**, 73–77 (2022).
42. Liu, C. et al. Tuning structural isomers of phenylenediammonium to afford efficient and stable perovskite solar cells and modules. *Nat. Commun.* **12**, 6394 (2021).
43. Ansari, F. et al. Passivation mechanism exploiting surface dipoles affords high-performance perovskite solar cells. *J. Am. Chem. Soc.* **142**, 11428–11433 (2020).
44. Zhao, L. et al. Chemical polishing of perovskite surface enhances photovoltaic performances. *J. Am. Chem. Soc.* **144**, 1700–1708 (2022).
45. Zhang, Z. et al. Carrier transport through the ultrathin silicon-oxide layer in tunnel oxide passivated contact (TOPCon) c-Si solar cells. *Sol. Energy Mater. Sol. Cells* **187**, 113–122 (2018).
46. Peibst, R. et al. Working principle of carrier selective poly-Si/c-Si junctions: is tunnelling the whole story? *Sol. Energy Mater. Sol. Cells* **158**, 60–67 (2016).
47. Stolterfoht, M. et al. Visualization and suppression of interfacial recombination for high-efficiency large-area pin perovskite solar cells. *Nat. Energy* **3**, 847–854 (2018).
48. Yang, S. et al. Stabilizing halide perovskite surfaces for solar cell operation with wide-bandgap lead oxysalts. *Science* **365**, 473–478 (2019).
49. Wang, Q., Dong, Q., Li, T., Gruverman, A. & Huang, J. Thin insulating tunneling contacts for efficient and water-resistant perovskite solar cells. *Adv. Mater.* **28**, 6734–6739 (2016).
50. Liang, C. et al. Two-dimensional Ruddlesden–Popper layered perovskite solar cells based on phase-pure thin films. *Nat. Energy* **6**, 38–45 (2020).
51. Proppe, A. H. et al. Synthetic control over quantum well width distribution and carrier migration in low-dimensional perovskite photovoltaics. *J. Am. Chem. Soc.* **140**, 2890–2896 (2018).
52. Westbrook, R. J. E. et al. 2D phase purity determines charge-transfer yield at 3D/2D lead halide perovskite heterojunctions. *J. Phys. Chem. Lett.* **12**, 3312–3320 (2021).
53. Green, M. A. The passivated emitter and rear cell (PERC): from conception to mass production. *Sol. Energy Mater. Sol. Cells* **143**, 190–197 (2015).
54. Zhang, F. et al. Metastable Dion–Jacobson 2D structure enables efficient and stable perovskite solar cells. *Science* **375**, 71–76 (2022).
55. Bertoluzzi, L. et al. Mobile ion concentration measurement and open-access band diagram simulation platform for halide perovskite solar cells. *Joule* **4**, 109–127 (2020).
56. Eames, C. et al. Ionic transport in hybrid lead iodide perovskite solar cells. *Nat. Commun.* **6**, 7497 (2015).
57. Thiesbrummel, J. et al. Universal current losses in perovskite solar cells due to mobile ions. *Adv. Energy Mater.* **11**, 2101447 (2021).
58. Gutierrez-Partida, E. et al. Large-grain double cation perovskites with 18 μs lifetime and high luminescence yield for efficient inverted perovskite solar cells. *ACS Energy Lett.* **6**, 1045–1054 (2021).
59. Dasgupta, A. et al. Visualizing macroscopic inhomogeneities in perovskite solar cells. *ACS Energy Lett.* **7**, 2311–2322 (2022).
60. Chen, C. et al. Arylammonium-assisted reduction of the open-circuit voltage deficit in wide-bandgap perovskite solar cells: the role of suppressed ion migration. *ACS Energy Lett.* **5**, 2560–2568 (2020).
61. Teale, S. et al. Dimensional mixing increases the efficiency of 2D/3D perovskite solar cells. *J. Phys. Chem. Lett.* **11**, 5115–5119 (2020).
62. Liu, Z. et al. In situ observation of vapor-assisted 2D–3D heterostructure formation for stable and efficient perovskite solar cells. *Nano Lett.* **20**, 1296–1304 (2020).
63. Lin, D. et al. Stable and scalable 3D–2D planar heterojunction perovskite solar cells via vapor deposition. *Nano Energy* **59**, 619–625 (2019).
64. Dualeh, A. et al. Effect of annealing temperature on film morphology of organic–inorganic hybrid perovskite solid-state solar cells. *Adv. Funct. Mater.* **24**, 3250–3258 (2014).
65. La-Placa, M. G. et al. Vacuum-deposited 2D/3D perovskite heterojunctions. *ACS Energy Lett.* **4**, 2893–2901 (2019).
66. Smith, I. C., Hoke, E. T., Solis-Ibarra, D., McGehee, M. D. & Karunadasa, H. I. A layered hybrid perovskite solar-cell absorber with enhanced moisture stability. *Ang. Chem. Int. Ed.* **53**, 11232–11235 (2014).
67. Emery, Q. et al. Encapsulation and outdoor testing of perovskite solar cells: comparing industrially relevant process with a simplified lab procedure. *ACS Appl. Mater. Interfaces* **14**, 5159–5167 (2022).
68. Zhu, H. et al. Long-term operating stability in perovskite photovoltaics. *Nat. Rev. Mater.* **8**, 569–586 (2023).
69. Brinkmann, K. O. et al. Suppressed decomposition of organometal halide perovskites by impermeable electron-extraction layers in inverted solar cells. *Nat. Commun.* **8**, 13938 (2017).
70. Hoffmann, L. et al. Spatial atmospheric pressure atomic layer deposition of tin oxide as an impermeable electron extraction layer for perovskite solar cells with enhanced thermal stability. *ACS Appl. Mater. Interfaces* **10**, 6006–6013 (2018).

71. Domanski, K. et al. Not all that glitters is gold: metal-migration-induced degradation in perovskite solar cells. *ACS Nano* **10**, 6306–6314 (2016).
72. Lin, Y. et al. Suppressed ion migration in low-dimensional perovskites. *ACS Energy Lett.* **2**, 1571–1572 (2017).
73. Huang, Z. et al. Suppressed ion migration in reduced-dimensional perovskites improves operating stability. *ACS Energy Lett.* **4**, 1521–1527 (2019).
74. Chen, R. et al. Reduction of bulk and surface defects in inverted methylammonium- and bromide-free formamidinium perovskite solar cells. *Nat. Energy* **8**, 839–849 (2023).
75. Luo, L. et al. Stabilization of 3D/2D perovskite heterostructures via inhibition of ion diffusion by cross-linked polymers for solar cells with improved performance. *Nat. Energy* **8**, 294–303 (2023).
76. Sutanto, A. A. et al. Dynamical evolution of the 2D/3D interface: a hidden driver behind perovskite solar cell instability. *J. Mater. Chem. A Mater.* **8**, 2343–2348 (2020).
77. Cho, J., Dubose, J. T., Le, A. N. T. & Kamat, P. V. Suppressed halide ion migration in 2D lead halide perovskites. *ACS Mater. Lett.* **2**, 565–570 (2020).
78. Wang, M. et al. Ammonium cations with high pKa in perovskite solar cells for improved high-temperature photostability. *Nat. Energy* **8**, 1229–1239 (2023).
79. Yang, W. S. et al. High-performance photovoltaic perovskite layers fabricated through intramolecular exchange. *Science* **348**, 1234–1237 (2015).
80. Jiang, Q. et al. Enhanced electron extraction using SnO_2 for high-efficiency planar-structure $\text{HC}(\text{NH}_2)_2\text{PbI}_3$ -based perovskite solar cells. *Nat. Energy* **2**, 16177 (2017).
81. Bi, D. et al. Polymer-templated nucleation and crystal growth of perovskite films for solar cells with efficiency greater than 21%. *Nat. Energy* **1**, 16142 (2016).
82. Tan, H. et al. Efficient and stable solution-processed planar perovskite solar cells via contact passivation. *Science* **355**, 722–726 (2017).
83. Zheng, X. et al. Defect passivation in hybrid perovskite solar cells using quaternary ammonium halide anions and cations. *Nat. Energy* **2**, 17102 (2017).
84. Cui, P. et al. Planar p-n homojunction perovskite solar cells with efficiency exceeding 21.3%. *Nat. Energy* **4**, 150–159 (2019).
85. Jeon, N. J. et al. A fluorene-terminated hole-transporting material for highly efficient and stable perovskite solar cells. *Nat. Energy* **3**, 682–689 (2018).
86. Jung, E. H. et al. Efficient, stable and scalable perovskite solar cells using poly(3-hexylthiophene). *Nature* **567**, 511–515 (2019).
87. Yang, D. et al. High efficiency planar-type perovskite solar cells with negligible hysteresis using EDTA-complexed SnO_2 . *Nat. Commun.* **9**, 3239 (2018).
88. Wang, L. et al. A Eu^{3+} – Eu^{2+} ion redox shuttle imparts operational durability to Pb-I perovskite solar cells. *Science* **363**, 265–270 (2019).
89. Li, N. et al. Cation and anion immobilization through chemical bonding enhancement with fluorides for stable halide perovskite solar cells. *Nat. Energy* **4**, 408–415 (2019).
90. Chen, Y. et al. Impacts of alkaline on the defects property and crystallization kinetics in perovskite solar cells. *Nat. Commun.* **10**, 1112 (2019).
91. Zhu, C. et al. Strain engineering in perovskite solar cells and its impacts on carrier dynamics. *Nat. Commun.* **10**, 815 (2019).
92. Kim, M. et al. Methylammonium chloride induces intermediate phase stabilization for efficient perovskite solar cells. *Joule* **3**, 2179–2192 (2019).
93. Chung, J. et al. Impact of electrode materials on process environmental stability of efficient perovskite solar cells. *Joule* **3**, 1977–1985 (2019).
94. Xu, Z. et al. A thermodynamically favored crystal orientation in mixed formamidinium/methylammonium perovskite for efficient solar cells. *Adv. Mater.* **31**, 1900390 (2019).
95. Niu, X. et al. Temporal and spatial pinhole constraints in small-molecule hole transport layers for stable and efficient perovskite photovoltaics. *J. Mater. Chem. A Mater. Chem.* **7**, 7338–7346 (2019).
96. Kim, H. et al. Optimal interfacial engineering with different length of alkylammonium halide for efficient and stable perovskite solar cells. *Adv. Energy Mater.* **9**, 1902740 (2019).
97. Abuhelaiqa, M. et al. Stable perovskite solar cells using tin acetylacetone based electron transporting layers. *Energy Environ. Sci.* **12**, 1910–1917 (2019).
98. Zheng, X. et al. Managing grains and interfaces via ligand anchoring enables 22.3%-efficiency inverted perovskite solar cells. *Nat. Energy* **5**, 131–140 (2020).
99. Xie, J. et al. Perovskite bifunctional device with improved electroluminescent and photovoltaic performance through interfacial energy-band engineering. *Adv. Mater.* **31**, 1902543 (2019).
100. Hang, P. et al. An interlayer with strong Pb–Cl bond delivers ultraviolet-filter-free, efficient, and photostable perovskite solar cells. *iScience* **21**, 217–227 (2019).
101. Wang, P. et al. Gradient energy alignment engineering for planar perovskite solar cells with efficiency over 23%. *Adv. Mater.* **32**, 1905766 (2020).
102. Zhang, L. et al. Side-chain engineering on dopant-free hole-transporting polymers toward highly efficient perovskite solar cells (20.19%). *Adv. Funct. Mater.* **29**, 1904856 (2019).
103. Zhang, Y. et al. Achieving reproducible and high-efficiency (>21%) perovskite solar cells with a presynthesized FAPbI_3 powder. *ACS Energy Lett.* **5**, 360–366 (2020).
104. Min, H. et al. Efficient, stable solar cells by using inherent bandgap of α -phase formamidinium lead iodide. *Science* **366**, 749–753 (2019).
105. Yoo, J. J. et al. Efficient perovskite solar cells via improved carrier management. *Nature* **590**, 587–593 (2021).
106. Peng, J. et al. Centimetre-scale perovskite solar cells with fill factors of more than 86 per cent. *Nature* **601**, 573–578 (2022).
107. Wu, S. et al. 2D metal–organic framework for stable perovskite solar cells with minimized lead leakage. *Nat. Nanotechnol.* **15**, 934–940 (2020).
108. Shen, C. et al. Stabilizing formamidinium lead iodide perovskite by sulfonyl-functionalized phenethylammonium salt via crystallization control and surface passivation. *Sol. RRL* **4**, 2000069 (2020).
109. Kim, G. et al. Impact of strain relaxation on performance of α -formamidinium lead iodide perovskite solar cells. *Science* **370**, 108–112 (2020).
110. Kim, M. et al. Conformal quantum dot- SnO_2 layers as electron transporters for efficient perovskite solar cells. *Science* **375**, 302–306 (2022).
111. Jeong, J. et al. Pseudo-halide anion engineering for α - FAPbI_3 perovskite solar cells. *Nature* **592**, 381–385 (2021).
112. Park, B. et al. Stabilization of formamidinium lead triiodide α -phase with isopropylammonium chloride for perovskite solar cells. *Nat. Energy* **6**, 419–428 (2021).
113. Chen, S., Xiao, X., Gu, H. & Huang, J. Iodine reduction for reproducible and high-performance perovskite solar cells and modules. *Sci. Adv.* **7**, eabe8130 (2021).
114. Min, H. et al. Perovskite solar cells with atomically coherent interlayers on SnO_2 electrodes. *Nature* **598**, 444–450 (2021).
115. Li, F. et al. Regulating surface termination for efficient inverted perovskite solar cells with greater than 23% efficiency. *J. Am. Chem. Soc.* **142**, 20134–20142 (2020).

116. Li, N. et al. Liquid medium annealing for fabricating durable perovskite solar cells with improved reproducibility. *Science* **373**, 561–567 (2021).
117. Jeong, M. et al. Stable perovskite solar cells with efficiency exceeding 24.8% and 0.3-V voltage loss. *Science* **369**, 1615–1620 (2020).
118. Zhang, T. et al. Ion-modulated radical doping of spiro-OMeTAD for more efficient and stable perovskite solar cells. *Science* **377**, 495–501 (2022).
119. Yang, G. et al. Stable and low-photovoltage-loss perovskite solar cells by multifunctional passivation. *Nat. Photon.* **15**, 681–689 (2021).
120. Wang, T. et al. Transporting holes stably under iodide invasion in efficient perovskite solar cells. *Science* **377**, 1227–1232 (2022).
121. Li, Z. et al. Organometallic-functionalized interfaces for highly efficient inverted perovskite solar cells. *Science* **376**, 416–420 (2022).
122. Park, J. et al. Controlled growth of perovskite layers with volatile alkylammonium chlorides. *Nature* **616**, 724–730 (2023).
123. Zhao, Y. et al. Inactive $(\text{PbI}_2)_2\text{RbCl}$ stabilizes perovskite films for efficient solar cells. *Science* **377**, 531–534 (2022).
124. Li, X. et al. Constructing heterojunctions by surface sulfidation for efficient inverted perovskite solar cells. *Science* **375**, 434–437 (2022).
125. Li, G. et al. Highly efficient p-i-n perovskite solar cells that endure temperature variations. *Science* **379**, 399–403 (2023).
126. Bai, Y. et al. Initializing film homogeneity to retard phase segregation for stable perovskite solar cells. *Science* **378**, 747–754 (2022).
127. Chen, T. et al. Inhibition of defect-induced α -to- δ phase transition for efficient and stable formamidinium perovskite solar cells. *Nat. Commun.* **14**, 6125 (2023).
128. Ye, S. et al. Expanding the low-dimensional interface engineering toolbox for efficient perovskite solar cells. *Nat. Energy* **8**, 284–293 (2023).
129. Li, H. et al. 2D/3D heterojunction engineering at the buried interface towards high-performance inverted methylammonium-free perovskite solar cells. *Nat. Energy* **8**, 946–955 (2023).
130. Li, F. et al. Hydrogen-bond-bridged intermediate for perovskite solar cells with enhanced efficiency and stability. *Nat. Photon.* **17**, 478–484 (2023).
131. Shi, P. et al. Oriented nucleation in formamidinium perovskite for photovoltaics. *Nature* **620**, 323–327 (2023).
132. Peng, W. et al. Reducing nonradiative recombination in perovskite solar cells with a porous insulator contact. *Science* **379**, 683–690 (2023).
133. Liu, X. et al. Perovskite solar cells based on spiro-OMeTAD stabilized with an alkylthiol additive. *Nat. Photon.* **17**, 96–105 (2022).
134. Xu, J. et al. Anion optimization for bifunctional surface passivation in perovskite solar cells. *Nat. Mater.* **22**, 1507–1514 (2023).
135. Yan, L. et al. Fabrication of perovskite solar cells in ambient air by blocking perovskite hydration with guanabenz acetate salt. *Nat. Energy* **8**, 1158–1167 (2023).
136. Li, Z. et al. Stabilized hole-selective layer for high-performance inverted p-i-n perovskite solar cells. *Science* **382**, 284–289 (2023).
137. Zhang, S. et al. Minimizing buried interfacial defects for efficient inverted perovskite solar cells. *Science* **380**, 404–409 (2023).
138. Liu, C. et al. Bimolecularly passivated interface enables efficient and stable inverted perovskite solar cells. *Science* **382**, 810–815 (2023).
139. Park, S. M. et al. Low-loss contacts on textured substrates for inverted perovskite solar cells. *Nature* **624**, 289–294 (2023).
140. Liang, Z. et al. Homogenizing out-of-plane cation composition in perovskite solar cells. *Nature* **624**, 557–563 (2023).
141. Huang, Z. et al. Anion- π interactions suppress phase impurities in FAPbI_3 solar cells. *Nature* **623**, 531–537 (2023).
142. Chen, W. et al. Interfacial stabilization for inverted perovskite solar cells with long-term stability. *Sci. Bull.* **66**, 991–1002 (2021).
143. Zhang, T. et al. Stable and efficient 3D–2D perovskite–perovskite planar heterojunction solar cell without organic hole transport layer. *Joule* **2**, 2706–2721 (2018).
144. Madhavan, V. E. et al. CuSCN as hole transport material with 3D/2D perovskite solar cells. *ACS Appl. Energy Mater.* **3**, 114–121 (2020).
145. Hu, S. et al. Optimized carrier extraction at interfaces for 23.6% efficient tin–lead perovskite solar cells. *Energy Environ. Sci.* **15**, 2096–2107 (2022).
146. Zhao, S. et al. General nondestructive passivation by 4-fluoroaniline for perovskite solar cells with improved performance and stability. *Small* **14**, e1803350 (2018).
147. Ye, F. et al. Overcoming C60-induced interfacial recombination in inverted perovskite solar cells by electron-transporting carborane. *Nat. Commun.* **13**, 7454 (2022).
148. You, S. et al. Bifunctional hole-shuttle molecule for improved interfacial energy level alignment and defect passivation in perovskite solar cells. *Nat. Energy* **8**, 515–525 (2023).
149. Zhu, H. et al. Tailored amphiphilic molecular mitigators for stable perovskite solar cells with 23.5% efficiency. *Adv. Mater.* **32**, 1907757 (2020).
150. Lin, R. et al. All-perovskite tandem solar cells with improved grain surface passivation. *Nature* **603**, 73–78 (2022).

Acknowledgements

We acknowledge: the HY-NANO project, which received funding from a European Research Council Starting Grant 2018 grant under the European Union’s Horizon 2020 research and innovation programme (grant agreement number 802862); the SPIKE project, which received funding from a European Research Council Proof of Concept 2022 grant under the European Union’s Horizon 2020 research and innovation programme (grant agreement number 101068936). G.G. acknowledges the GOPV project (CSEAA_00011), which received funds from Bando Ricerca di Sistema—CSEA—TIPO A Piano triennale 2019–2021 Decreto direttoriale 27 Ottobre 2021 del Ministero della Transizione Ecologica; MASE-(ex MITE); and Ministero dell’Università e della Ricerca and University of Pavia through the programme Dipartimenti di Eccellenza 2023–2027. This research was made possible by a US Department of the Navy Office of Naval Research Grant (N00014-20-1-2572). This work was supported in part by the Ontario Research Fund’s Research Excellence programme (ORF7; Ministry of Research and Innovation, Ontario Research Fund; Research Excellence Round 7). S.T. was supported by the Hatch Scholarship for Sustainable Energy Research.

Author contributions

M.D. and S.T. performed the literature review and contributed equally to writing the paper. B.C. contributed to discussion of the idea and revision of the manuscript. E.H.S. and G.G. conceived of the idea and supervised the work.

Competing interests

The authors declare no competing interests.

Additional information

Supplementary information The online version contains supplementary material available at <https://doi.org/10.1038/s41560-024-01529-3>.

Correspondence and requests for materials should be addressed to Edward H. Sargent or Giulia Grancini.

Peer review information *Nature Energy* thanks Yi-Bing Cheng and the other, anonymous, reviewer(s) for their contribution to the peer review of this work.

Reprints and permissions information is available at
www.nature.com/reprints.

Publisher's note Springer Nature remains neutral with regard to jurisdictional claims in published maps and institutional affiliations.

Springer Nature or its licensor (e.g. a society or other partner) holds exclusive rights to this article under a publishing agreement with the author(s) or other rightsholder(s); author self-archiving of the accepted manuscript version of this article is solely governed by the terms of such publishing agreement and applicable law.

© Springer Nature Limited 2024, corrected publication 2024